

Characterization of UV detectors at SURF III (invited)

Ping-Shine Shaw,^{a)} Thomas C. Larason, Rajeev Gupta, and Keith R. Lykke
National Institute of Standards and Technology, Gaithersburg, Maryland 20899

(Presented on 23 August 2001)

The Synchrotron Ultraviolet Radiation Facility (SURF III) at the National Institute of Standards and Technology provides a unique research opportunity in precision measurements with its continuous and calculable radiation stretching from the soft x ray to the far infrared. In response to the rapid development of ultraviolet photodetectors for applications ranging from industrial photolithography to astrophysics, we have developed measurement capabilities to characterize photodetectors with high accuracy. The absolute measurements at SURF III are based on a high-accuracy liquid-helium cooled cryogenic radiometer for measuring the power of the dispersed radiation from SURF III through a monochromator. Typical detector calibration uncertainties achieved at SURF III using cryogenic radiometer is better than 0.5% in the ultraviolet. Equipped with such a tool, we were able to study a variety of ultraviolet detectors and determine their spectral responsivities, surface reflectivities, and the effects of radiation damage. Due to the accuracy of these measurements, the internal quantum efficiencies of the photodetectors can be derived and theoretically modeled to provide information on the mechanism of photo detection. © 2002 American Institute of Physics. [DOI: 10.1063/1.1445825]

I. INTRODUCTION

The Synchrotron Ultraviolet Radiation Facility (SURF III)¹ at the National Institute of Standards and Technology (NIST) is dedicated to setting the radiation measurement standards for radiometry. Because of the relatively low electron energy and highly uniform magnetic field of the storage ring, SURF III is especially suitable for UV measurements with high accuracy. Beamline 4,^{2,3} operated by the Optical Technology Division, is one of the SURF III radiometric beamlines for UV detector characterization that covers the spectral range from the visible down to about 130 nm. UV detectors in this range have important technological applications, such as medical procedures, UV curing, and semiconductor photolithography where intense research and development efforts are underway for the use of 193 and 157 nm lasers as light sources.⁴ New UV detectors are constantly being developed to address issues such as radiation damage, solar blindness, linearity, and spatial and time resolution. The purpose of beamline 4 is to characterize UV detectors with an emphasis on absolute and accurate measurements. This is achieved by establishing an UV scale through a high-accuracy absolute cryogenic radiometer (ACR). The UV scale on beamline 4 enables measurement of detector spectral responsivity with an uncertainty as low as 0.5%.³ The low uncertainty achieved for detector calibration forms the basis for further detector characterization.

In addition to detector calibration, the end station of beamline 4 can also measure quantities such as spatial uniformity, radiation damage, and detector surface reflectivity at specific angles of incidence. The results of all these measurements performed on beamline 4 provide practical information in applying the detector under test for specific applica-

tions. In addition, the data generate insights into the detector's internal photon detection mechanism. For example, with the measured detector spectral responsivity and surface reflectance, the internal quantum efficiency, defined as the number of electrons generated per absorbed photon, can be derived. The internal quantum efficiency of a detector as a function of wavelength in turn can be modeled for the depth profile of charge collection efficiency. This article describes various measurement methods for detector characterization with examples to demonstrate the capability of beamline 4.

II. BEAMLINE DESCRIPTION

Beamline 4 consists of two grazing-incidence mirrors, a 2-m-normal incidence monochromator (NIM) and an imaging system downstream of the monochromator. The schematic diagram of the beamline 4 components is shown in Fig. 1. The ACR connected at the very end of the beamline

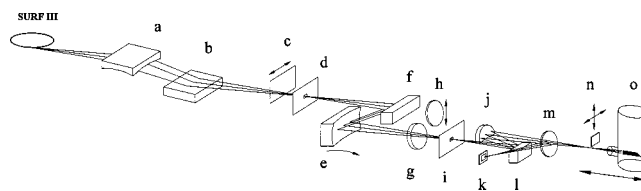


FIG. 1. Schematic diagram of beamline 4 for UV radiometry at the Synchrotron Ultraviolet Radiation Facility (SURF III) showing grazing incidence preoptics (a) and (b), shutter (c), monochromator entrance slit (d), grating (e), plane mirror (f), CaF₂ window (g), quartz filter (h), monochromator exit slit (i), spherical mirror (j), monitor photodiode (k), plane mirror (l), CaF₂ beam splitter (m), test detector (n), and absolute cryogenic radiometer (ACR) (o).

^{a)}Electronic mail: shaw@nist.gov

measures the incident radiant power by using electrical substitution at liquid helium temperature^{5,6} and serves as the primary standard for detector responsivity measurements. Cryogenic radiometers are the most accurate radiant power detectors currently available and are widely established at national laboratories as primary standards. At beamline 4, the typical uncertainty is 0.2% for power measurement by the ACR. A detailed discussion of the beamline 4 components, the UV scale establishment by the ACR, and an uncertainty analysis was given elsewhere.^{2,3} Here, we only give a brief description of measurement configurations for test detectors.

The test detector is placed inside the detector chamber and mounted on an x - y translation stage and a rotation stage. The linear motions are used to raster scan the test detector for spatial response mapping and the rotation stage is used to set the incidence angle of the radiation on the test detector. The reflected light from the test detector is measured by a second calibrated photodiode placed inside the detector chamber facing the test detector photodiode. Care was taken so that the reflected light from the reflectance-measurement photodiode does not go back to the test diode and interfere with the responsivity measurement of the test detector. The signals from the test detector and the reflectance-measurement photodiode are simultaneously recorded using a computer. All measurements from both detectors are normalized by a monitor diode upstream of the beamline to eliminate the effects of the gradual decay of the electron beam in the storage ring and any fluctuations of the beam.

To induce radiation damage on a test detector, we used either the monochromatized radiation from beamline 4 or an external UV source such as a 157-nm-excimer laser. The radiation from beamline 4 is somewhat lower in power ($\sim 1 \mu\text{W}$) but can be useful at shorter wavelengths. For the 157 nm laser, an UV window port on the side of the detector chamber allows the laser beam to enter the detector chamber and irradiate the test detector. After irradiation, the spectral responsivity of the test detector can be measured and compared with the spectral responsivity prior to irradiation.

III. DETECTOR CALIBRATION

The calibration of the spectral power responsivity of a detector measured on beamline 4 has units of A/W. The current from the detector is measured by a precision picoammeter and the power of incident radiation is measured indirectly by the ACR. We have calibrated a variety of UV detectors currently available using beamline 4 as part of our effort to find stable detectors that are candidates for better UV working standards. A UV working standard detector at NIST is calibrated against the primary standard and subsequently used for routine calibration of other detectors. For UV, the working standard must have good radiation hardness, spatially uniform responsivity, and low noise. Figure 2 shows the spectral power responsivity of several photodiodes including: UV Si p -on- n (Hamamatsu 5227), SiC, and GaN (APA) photodiodes.⁷ The typical measurement uncertainty is less than 0.5% for 157 and 193 nm excimer laser lines that are of the most interest to the UV photolithography industry.

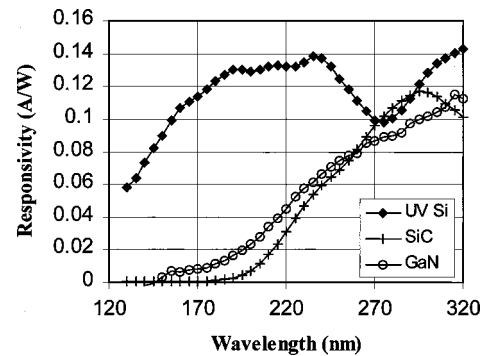


FIG. 2. Measured UV spectral responsivities of three photodiodes, UV Si p -on- n , SiC, and GaN.

IV. RADIATION DAMAGE

One of the major challenges for UV detector metrology is the change in detector responsivity caused by high-energy photons or particles. Radiation damage of detectors is a concern when the detectors are used to monitor wafer-plane dosage of UV laser radiation in photolithography.

It is well known that the standard Si p - n junction photodiode is prone to radiation damage for wavelengths as long as 250 nm.⁸ Recently, a number of photodiodes were developed to improve the radiation hardness of Si photodiodes. These improved detectors include photodiodes with n - p junction, nitrided SiO₂ window layer, and the replacement of the top SiO₂ window layer with more inert materials like PtSi.⁹

We have studied the radiation damage effect for several different types of photodiodes with a 157-nm-excimer laser.¹⁰ The 157 nm laser was used to induce radiation damage and beamline 4 radiation was used as a probe beam to monitor the change of the detector spectral responsivity. Figure 3 shows the change in responsivity at 157 nm as a function of the dosage for three types of Si photodiodes: UV Si p -on- n , nitrided Si, and Si photodiode with PtSi front window. The effect of radiation damage is clearly demonstrated in Fig. 4 where a spatial uniformity scan was performed at 157 nm on a Si photodiode that was subjected to a total dose of 1 J/cm^2 of 157 nm laser pulses.

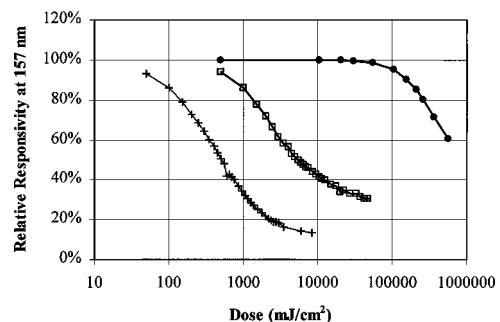


FIG. 3. Radiation damage of three types of Si photodiodes, UV Si p -on- n (crosses), nitrided Si (squares), and Si photodiode with PtSi front window (circles), by a pulsed 157-nm-excimer laser.

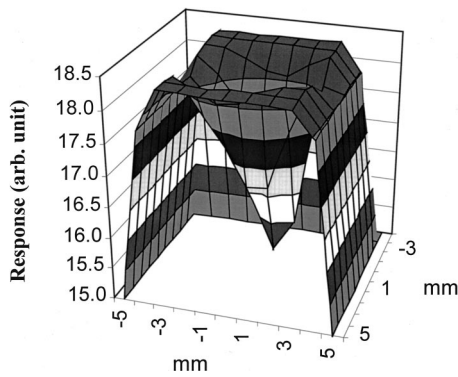


FIG. 4. Spatial responsivity of a photodiode damaged by a 157-nm-laser measured at 157 nm.

V. DETECTOR REFLECTANCE AND INTERNAL QUANTUM EFFICIENCY

The end station of beamline 4 can be easily adapted for detector reflectance measurements, similar to a reflectometer, with an additional photodiode to measure the reflected light from the test detector. The angle of incidence can be adjusted to an accuracy of $\pm 1^\circ$. With this setup, both the detector spectral responsivity and reflectance can be measured. Figure 5 shows the result of such a measurement for a Si photodiode with a PtSi front window.

With the measured spectral responsivity and reflectance of a detector, the detector internal quantum efficiency $Q_{\text{int}}(\lambda)$, in number of electron per absorbed photon, can be readily calculated:

$$Q_{\text{int}}(\lambda) = \frac{S(\lambda)}{1-r(\lambda)} \cdot \left(\frac{hc}{\lambda} \cdot \frac{1}{q} \right),$$

where $S(\lambda)$ is the spectral responsivity in A/W, $r(\lambda)$ is the detector reflectance, hc/λ is the energy of a photon in Joules, and q is the charge of the electron in Coulombs.

The internal quantum efficiency renders its importance for typical modern Si photodiodes because of the near 100%

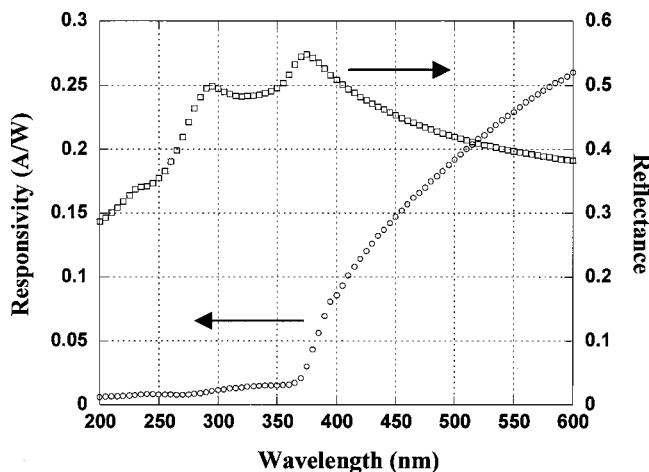


FIG. 5. Responsivity and reflectivity of a Si photodiode with PtSi front window measured at beamline 4 with an incidence angle of 10 degrees.

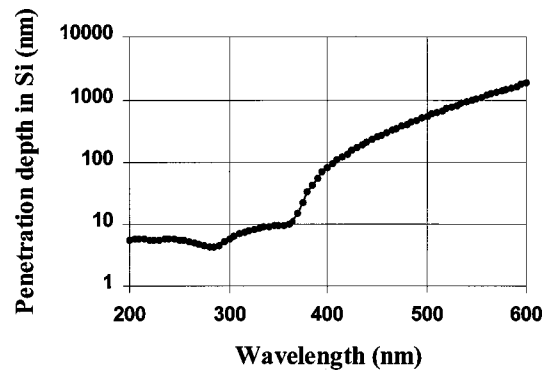


FIG. 6. Penetration depth for silicon crystal as a function of wavelength.

value throughout the visible to near ultraviolet. This effect, also known as the self-calibration of Si photodiodes,^{11,12} is one of the foundations for detector-based radiometry using Si photodiodes.⁵ Beyond the near ultraviolet and on to the x-ray region, the internal quantum efficiency increases roughly proportional to the photon energy because of the impact ionization from excess photon energy.¹³ The near 100% internal quantum efficiency in the visible and near ultraviolet indicates very efficient conversion of photons to electron-hole pairs and the collection of electrons to the external circuit inside the photodiode. This is not the case for photodiodes fabricated with defects or trap states and the internal quantum efficiency will clearly indicate such problems.

In addition, it is of interest to note that the penetration depth into a silicon substrate is a strong function of the wavelength, even in the wavelength range from the near ultraviolet to the visible. As shown in Fig. 6,¹⁴ the penetration depth in silicon changes more than two orders of magnitude from 300 to 600 nm. Such an effect suggests that scanning the wavelength in this region constitutes a tool for depth profiling of a silicon photodiode. Similar effects can only be found by using x rays with a comparable penetration depth. However, the use of x rays to probe a silicon photodiode is complicated by higher quantum efficiency from impact ion-

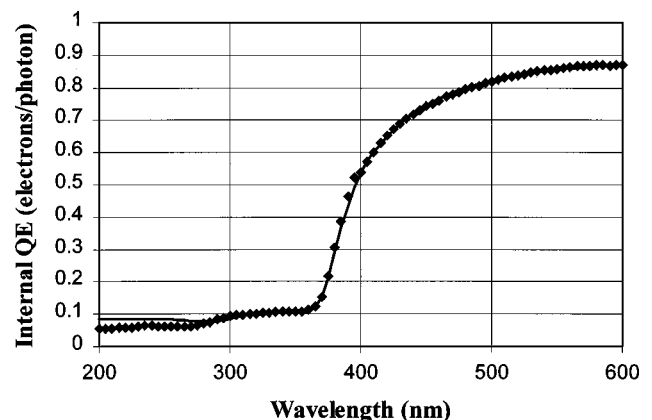


FIG. 7. Internal quantum efficiency of a Si photodiode with PtSi front window derived from the data of Fig. 5 (diamonds). The line is the simulated internal quantum efficiency based on a modeled charge collection efficiency as a function of the depth inside the photodiode.

ization and possible damage of the photodiode due to the higher energy of the x-ray photons.

As an example, we derived the internal quantum efficiency of a Si photodiode with a PtSi front window from the data in Fig. 5. The result is shown in Fig. 7, where a sharp drop in the internal quantum efficiency for wavelengths shorter than 400 nm is shown. This indicates that a shallow region, less than 100 nm deep near the surface (see Fig. 6), has a very low charge collection efficiency. This supports the existence of trap states at the interface between the PtSi front window and the silicon substrate underneath. Furthermore, the charge collection efficiency as a function of depth can be modeled⁵ based on the measured internal quantum efficiency. The convolution of the modeled charge collection efficiency and the penetration depth shown in Fig. 6 is used to simulate the internal quantum efficiency of the photodiode. The result of such a simulation for the PtSi front window Si photodiode is shown in Fig. 7 (solid line) along with the measured internal quantum efficiency (diamonds). The simulated charge collection efficiency also shows very low collection efficiency around the first 10 nm and gradually increases to close to 100% at a depth of around 100 nm. Details of this simulation will be reported in the near future.¹⁵

ACKNOWLEDGMENT

The authors would like to thank the SURF staff members for their help in operating SURF III for this work.

¹U. Arp, R. Friedman, M. L. Furst, S. Makar, and P. S. Shaw, *Metrologia* **37**, 357 (2000).

²P. S. Shaw, K. R. Lykke, R. Gupta, T. R. O'Brian, U. Arp, H. H. White, J. L. Dehmer, and A. C. Parr, *Appl. Opt.* **38**, 18 (1999).

³P. S. Shaw, T. C. Larason, R. Gupta, S. W. Brown, R. E. Vest, and K. R. Lykke, *Rev. Sci. Instrum.* **72**, 2242 (2001).

⁴C. L. Cromer, T. B. Lucatoro, T. R. O'Brian, and M. Walhout, *Solid State Technol.* **39**, 75 (1996).

⁵T. R. Gentile, J. M. Houston, and C. L. Cromer, *Appl. Opt.* **35**, 4392 (1996).

⁶T. R. Gentile, J. M. Houston, J. E. Hardis, C. L. Cromer, and A. C. Parr, *Appl. Opt.* **35**, 1056 (1996).

⁷Certain commercial equipment, instructions, or materials are identified in this article to foster understanding. Such identification does not imply recommendation or endorsement by the National Institute of Standards and Technology, nor does it imply that the materials or equipment identified are necessarily the best available for the purpose.

⁸L. Werner, *Metrologia* **35**, 407 (1998).

⁹R. Korde, J. S. Cable, and L. R. Canfield, *IEEE Trans Nucl. Sci.* **40**, 1655 (1993).

¹⁰R. Gupta, P. S. Shaw, and K. R. Lykke (unpublished).

¹¹J. Geist and H. Baltes, *Appl. Opt.* **28**, 3929 (1989).

¹²J. Geist, *Appl. Opt.* **18**, 760 (1979).

¹³F. Scholze, H. Rabus, and G. Ulm, *J. Appl. Phys.* **84**, 2926 (1998).

¹⁴E. D. Palik, *Handbook of Optical Constants of Solids* (Academic, New York, 1985).

¹⁵P. S. Shaw (unpublished).